Effects of Ageing Treatment on Microstructures and Mechanical Properties of a Near-β Ti Alloy

Song Zhang , Y.C. Lin * , Li-Hua Wang , Hong-Bo Ding , Yu-Liang Qiu

Posted Date: 3 January 2024

doi: 10.20944/preprints202401.0281.v1

Keywords: Ti alloy; ageing treatment; microstructures; mechanical properties; fracture mechanisms

Article

Effects of Ageing Treatment on Microstructures and Mechanical Properties of a near-β Ti Alloy

Song Zhang [1], Y.C. Lin [1,2,3,*], Li-Hua Wang [1], Hong-Bo Ding [2,4] and Yu-Liang Qiu [5]

[1] Light Alloy Research Institute, Central South University, Changsha 410083, China; 203801010@csu.edu.cn (S.Z.); 931180189@qq.com (L.-H.W.)
[2] School of Mechanical and Electrical Engineering, Central South University, Changsha 410083, China; ding_cnpt@163.com (H.-B.D.)
[3] State Key Laboratory of Precision Manufacturing for Extreme Service Performance, Changsha 410083, China
[4] China Nonferrous Metals Processing Technology Co. LTD, Luoyang 471039, China
[5] Rongcheng Huadong Metal-forming Machinery Co. LTD, Rongcheng 264300, China
* Correspondence: yclin@csu.edu.cn

Abstract: In the present work, the effects of ageing treatment on the microstructures of a near-β Ti alloy (TC18) are studied. The influence of ageing treatment on the tensile properties and failure mechanisms are systematically analyzed. It is found that the size and morphology of the primary α (α_p) phases are insensitive to ageing temperature and time. Furthermore, the ageing temperature and time dramatically influence the precipitation of the secondary α (α_s) phases. Massive α_s phases precipitate and gradually coarsen, and finally weave together with increasing the ageing temperature or extending the ageing time. The thickness of α_s phases is responsible for the material strengths, while the content of α phases can enhance the material ductility. The ductile characteristics of the alloy with coarser α_s phases are more obvious than those with thinner α_s phases. Therefore, the ageing treatment is helpful for the precipitation and homogeneous distribution of α_s phases, which is essential for balancing the strengths and ductility of the studied Ti alloy.

Keywords: Ti alloy; ageing treatment; microstructures; mechanical properties; fracture mechanisms

1. Introduction

Near β-Ti alloys such as Ti-10V-2Fe-3Al, Ti-5Al-5V-5Mo-3Cr and Ti-5Al-5Mo-5V-1Cr-1Fe (TC18) have been widely used in the aeronautical industry in virtue of excellent performances in strength, toughness and corrosion resistance [1–5]. In general, the relationship between the desired microstructures and excellent mechanical properties of Ti alloys is inextricable, and the properties can be adjusted by tailoring the proportions or morphologies of α or β phases using heat treatment [6–10]. Hence, the diversity of microstructures and the complex influence of microstructure on properties in Ti alloys have stimulated ever-increasing research interests [11–17].

Usually, α phases are crucial to balance the mechanical properties such as the strength and ductility of Ti alloys [18–20]. Duplex microstructures possess both good ductility and high strengths compared with other typical microstructures (equiaxed, widmannstatten and basket-weave microstructures) [21–25]. The duplex microstructures can be induced by typical thermo-mechanical paths, in particular the ageing conditions. Therefore, in recent decades, some researches have been contributed to obtaining these considerable microstructures of Ti alloys by solution plus ageing treatment. Solution plus single ageing was usually used by some researchers who found that the α_p are highly sensitive to the solution temperature, while the α_s phases are greatly affected by ageing conditions. Moreover, the precipitation of α_s phases could significantly enhance the properties of Ti alloys [26–29]. Also, the uniform and ultra-fine α_s phases were obtained by solution plus duplex ageing [30]. In recent years, the multi-stage treatment methods were employed to optimize the mechanical properties of Ti alloys [31]. It is indicated that the content of α_p phase is relatively stable after the multi-stage treatment, while the size of α_s phase becomes non-uniform and the content of α_s phase increases with increasing cooling rate. Besides, the influence of aged microstructures on

Preprints (www.preprints.org) | NOT PEER-REVIEWED | Posted: 3 January 2024 doi:10.20944/preprints202401.0281.v1

mechanical properties was investigated. Guo et. al. [15] demonstrated that the strength of TC4-DT alloy with duplex microstructures is minimally impacted by α_p phase, while the ductility significantly increases as the content of α_p phase increases. In other words, α_s phases are vital for improving the strength and ductility. Also, the α_p phase can improve the fracture toughness by changing the crack propagation paths and augmenting energy consumptions [32]. Aeby-Gautier et al. [33] examined that the formation of α_s phase during ageing can increase the tensile strength. Hence, the tailoring of α_p and α_s phases is the key to obtain the excellent properties of Ti alloys with duplex microstructures.

Nevertheless, the previous researchers have devoted to elaborating the influence of heating paths on the morphologies and properties of phases. But, less attention was paid to the quantitative characterization of α_p and α_s phases in aged near β-Ti alloys. Furthermore, the relationship between the content/size of phase and tensile properties is also inexplicit. The quantitative relation has also not been directly testified by experimental evidences under different ageing conditions. Especially, the evolution law of α_s phases and mechanical properties under different ageing conditions are less involved. Therefore, the influences of ageing conditions on the content and morphologies of α_p and α_s phases in a near β-Ti alloy (TC18) are analyzed. The effects of crucial microstructure features on mechanical properties are also discussed. Subsequently, the tensile failure mechanisms are revealed. These experimental findings and understandings are useful to improve the performance of TC18 alloy.

2. Material and Experiment Procedures

The chemical compositions (wt. %) of the studied TC18 alloy are presented as follows: 5.16 Al, 4.92 Mo, 4.94 V, 1.10 Cr, 0.98 Fe and balance Ti. The transition temperature of full β phase is 875±5 °C. The original microstructures are presented in Figure 1a,b. There are some discontinuous grain boundary α phases (α_{GB}), α_p phases, α_s phases and β matrix (β_m). All specimens were pretreated at 780 °C for 1 h, then cooled by water quenching (WQ) before ageing. The pretreated microstructure is displayed in Figure 1c, and Figure 1d shows the size distribution of α_p phases.

To explore the effects of ageing conditions on microstructures and properties, several heat treatment paths were designed, and an air cooling (AC) method was performed after ageing treatment, as presented in Table 1. The specimens for metallographic examination were cut into slices using electrical discharge machining. The section of each specimen was prepared using the standard metallurgical procedures. The specimens were firstly abraded by SiC paper from grid 400# to 2000# and polished with Al_2O_3 suspension liquid, and then etched in a solution mixed by 2% HF, 5% HNO_3 and 93% H_2O [5]. In order to carry out transmission electron microscopy (TEM) observation, the thin foils were firstly ground by SiC paper and polished using the twin jet electrochemical polishing in a solution of 5% perchloric acid, 35% normal butanol and 60% methanol. The microstructure and fracture morphologies were characterized by scanning electron microscopy (SEM) technique. The TEM figures were captured by the Tecnai G2-20 microscope. Subsequently, the software of Image-pro plus 6.0 was employed to measure the content, grain diameters and the thickness of phases. The tensile specimens with a gauge length of 30 mm and a diameter of 6 mm were prepared and then polished with 400-1000# grid SiC paper. The tensile tests were performed in the MTS-GWT2105 test machine.

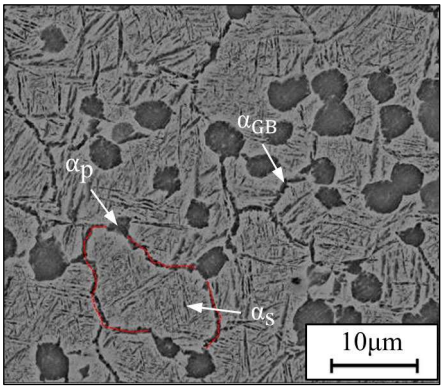

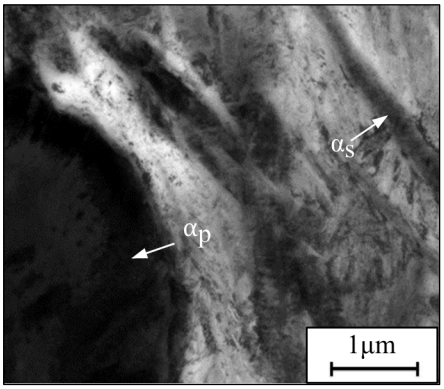

Preprints (www.preprints.org) | NOT PEER-REVIEWED | Posted: 3 January 2024 doi:10.20944/preprints202401.0281.v1

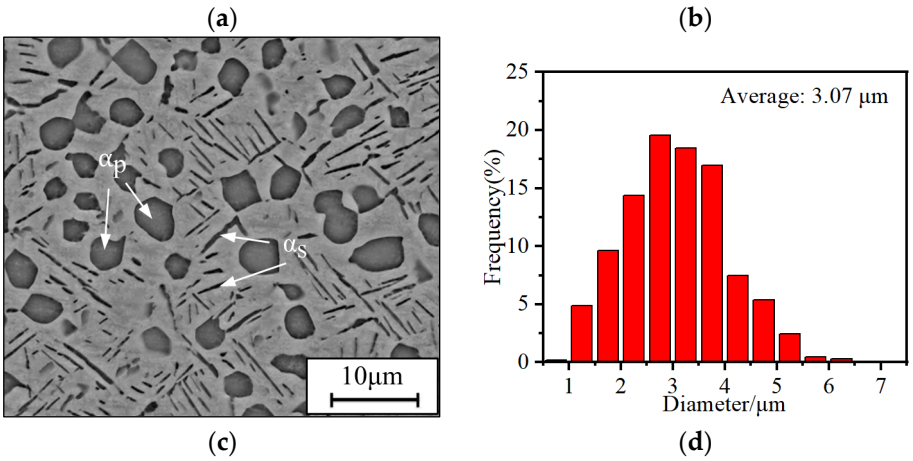

Figure 1. Microstructures of as-received alloy: (**a**) SEM observation; (**b**) TEM observation (bright field); (**c**) SEM observation (pretreated); (**d**) Particle size distribution of α_p phases (pretreated).

Table 1. Experimental schemes for heat treatment.

Route No.	Pretreatment	Ageing Condition		
		Temperature (°C)	Hold Time (h)	Cooling Method
1	780 °C/1h/WQ	400	4	AC
2		450		
3		500		
4		550		
5		600		
2-1		450	1	
2-2		450	2	
2-3		450	8	

3. Results and Discussions

3.1. Effects of Ageing Conditions on Microstructures

3.1.1. Effects of ageing temperature

Figure 2 illustrates the influence of ageing temperature on the microstructures and the size distribution of α_p phases. The α_p phases mainly distribute at β grain boundaries, and the size of β grain is only a few tens of microns. It indicates that there is a pinning effect induced by α_p phases on the growth of β grain during ageing treatment (Figure 2a,c,e,g). With increasing the temperature, the size uniformity of α_p phase gradually decreases but the average size slightly increases. The average sizes of α_p phase have been estimated to be 3.11 μm, 3.13 μm, 3.18 μm and 3.24 μm (Figure 2b,d,f,h), respectively, when the alloy was aged at 450 °C, 500 °C, 550 °C and 600 °C. The average size of α_p phase is less than 3.3 μm and the growth of α_p phase is restricted during ageing treatment. In the ageing process, the transformation of metastable β phases to α phases is dominated by the element diffusion. Therefore, the precipitation of α_s phases is slow owing to the low driving force at lower temperatures. The α_s phases precipitate not only at α/β interface, but also within β_m. The precipitation is dominated by increasing the diffusion driving force as the temperature is increased [34]. In summary, the effects of temperature on α_p phases are negligible because the metastable β phases mainly transform to α_s phases during the ageing treatment.

Preprints (www.preprints.org) | NOT PEER-REVIEWED | Posted: 3 January 2024 doi:10.20944/preprints202401.0281.v1

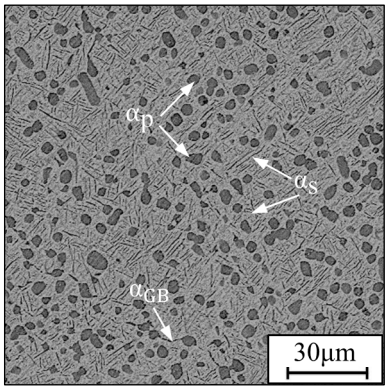

(a)

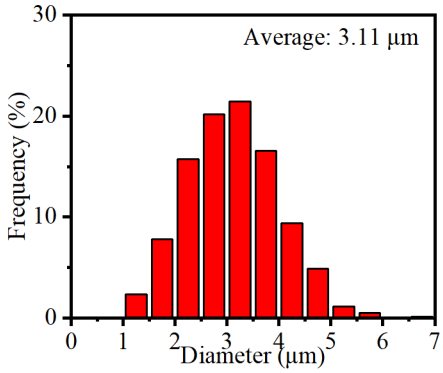

(b)

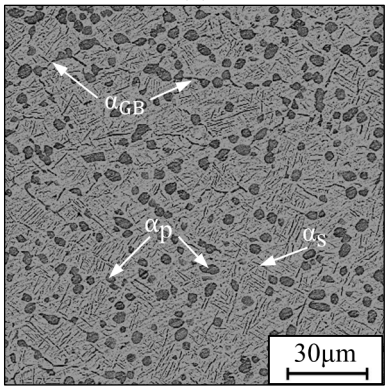

(c)

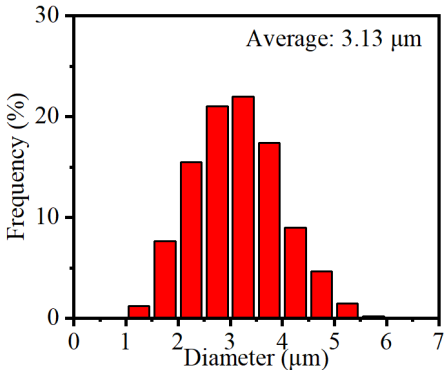

(d)

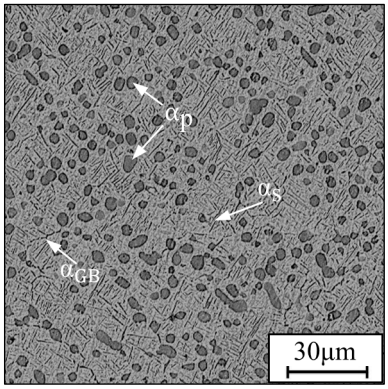

(e)

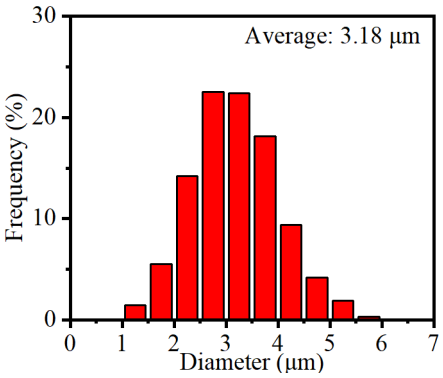

(f)

Preprints (www.preprints.org) | NOT PEER-REVIEWED | Posted: 3 January 2024 doi:10.20944/preprints202401.0281.v1

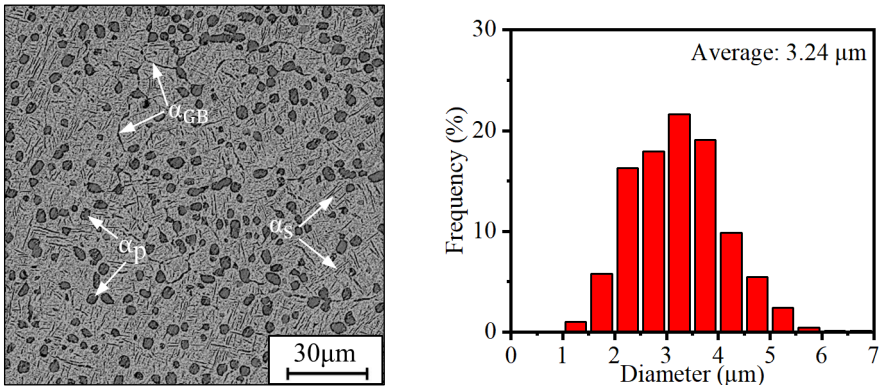

(g) (h)

Figure 2. Microstructures and the size distribution of α_p phases of TC18 alloy aged at: (**a–b**) 450 °C; (**c–d**) 500 °C; (**e–f**) 550 °C; (**g–h**) 600 °C.

Figure 3 shows the influence of ageing temperature on the formation of α_s phases. A few dislocations and substructures are found. The precipitated α_s phases are cross-distributed irregularly and their thickness vary from 0.2 to 0.6 μm. Also, the orientations of the precipitated α_s phases are random [35]. As illustrated in Figure 3a, α_s phases with a fine acicular shape precipitate and several unaged areas appear in the β_m at the ageing temperature of 400 °C. Meanwhile, the distinguishing α_s phases from β_m are tricky because the boundaries of α_s phases are blurred. Due to the high content of β-stable elements in β_m and a smaller driving force for solute atom diffusion at lower ageing temperatures, the transformation for β_m to α_s phases is insufficient (Figure 3a). Therefore, the content of α_s phases is extremely low, and the average thickness is small at lower ageing temperatures. As the temperature is increased, the massive α_s phases precipitate in a complete ageing process (Figure 3b–d). Moreover, the α_s phases coarsen and tightly weave together. The α_s/β interfaces are visible especially at high ageing temperatures such as 600 °C, and the average thickness of α_s phases increases to about 0.47 μm (Table 2). So, α_s phases are sensitive to the variations of ageing temperature, and the coarsening rate of α_s phases is obviously affected by the diffusivity of solute atoms [36].

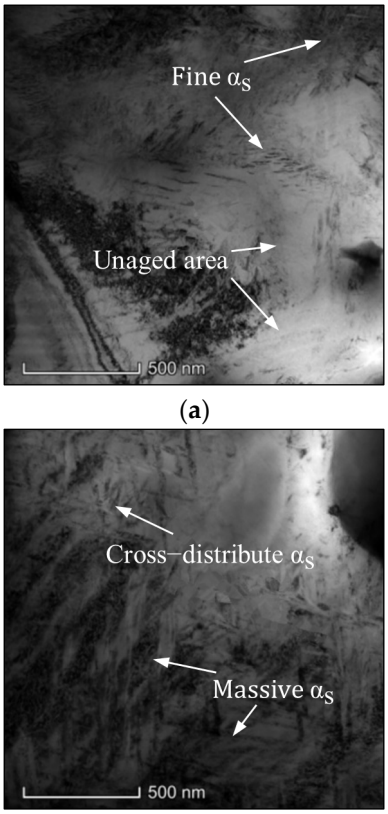

(a)

Preprints (www.preprints.org) | NOT PEER-REVIEWED | Posted: 3 January 2024 doi:10.20944/preprints202401.0281.v1

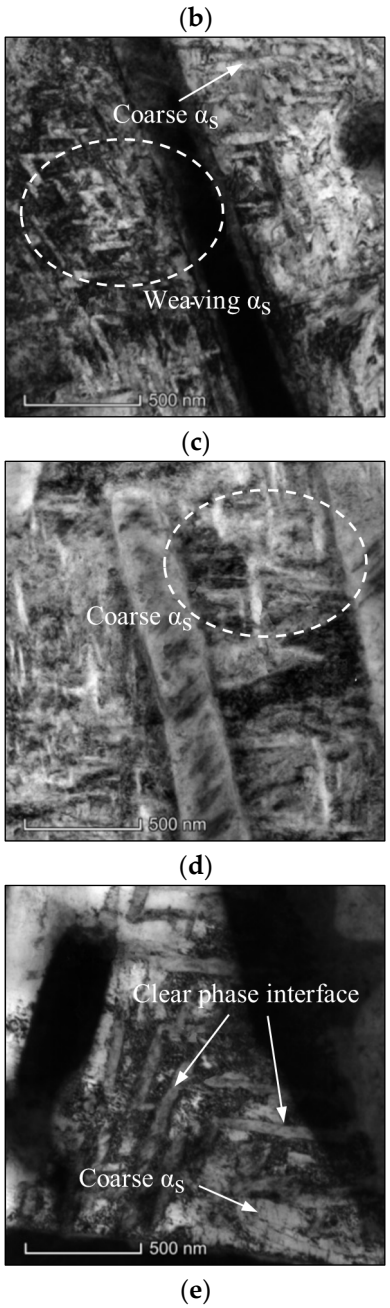

Figure 3. TEM micrographs of TC18 alloy aged at: (**a**) 400 °C; (**b**) 450 °C; (**c**) 500 °C; (**d**) 550 °C; (**e**) 600 °C.

Table 2. Content and size of phases with different ageing conditions.

Ageing Condition [d]	The content of α phases (%)	The content of α_p phases (%)	The diameter of α_p phases (μm)	The content of α_s phases (%)	The thickness of α_s phases (μm)
450 °C	27.61	18.34	3.11	9.27	0.30
500 °C	23.79	16.87	3.13	6.92	0.35
550 °C	27.01	18.56	3.18	8.45	0.45
600 °C	25.89	18.57	3.24	7.32	0.47

[d] Ageing time of 4h and subsequent AC.

3.1.2. Effects of Ageing Time

Figure 4 illustrates the influence of ageing time on the microstructures and the particle size distribution of α_p phase when the alloy was aged at 450 °C. As shown in Figure 4a–c, there are

Preprints (www.preprints.org) | NOT PEER-REVIEWED | Posted: 3 January 2024 doi:10.20944/preprints202401.0281.v1

spherical α phases, α_{GB} and β transition phases. With prolonging the ageing time, the variations of α_p phases are inconspicuous. The particle size distribution and average size of α_p phases at different ageing time are shown in Figure 4d–f. The average size and content of α_p phase fluctuate only slightly with increasing the time, and the average sizes are 3.15, 3.11 and 3.04 μm, respectively, when the ageing time are 1, 4 and 8 h. The content of α_p phases shows an opposite pattern, which first decreases and then increases, and the corresponding contents of α_p phases are 16.35%、18.34% and 16.53%, respectively.

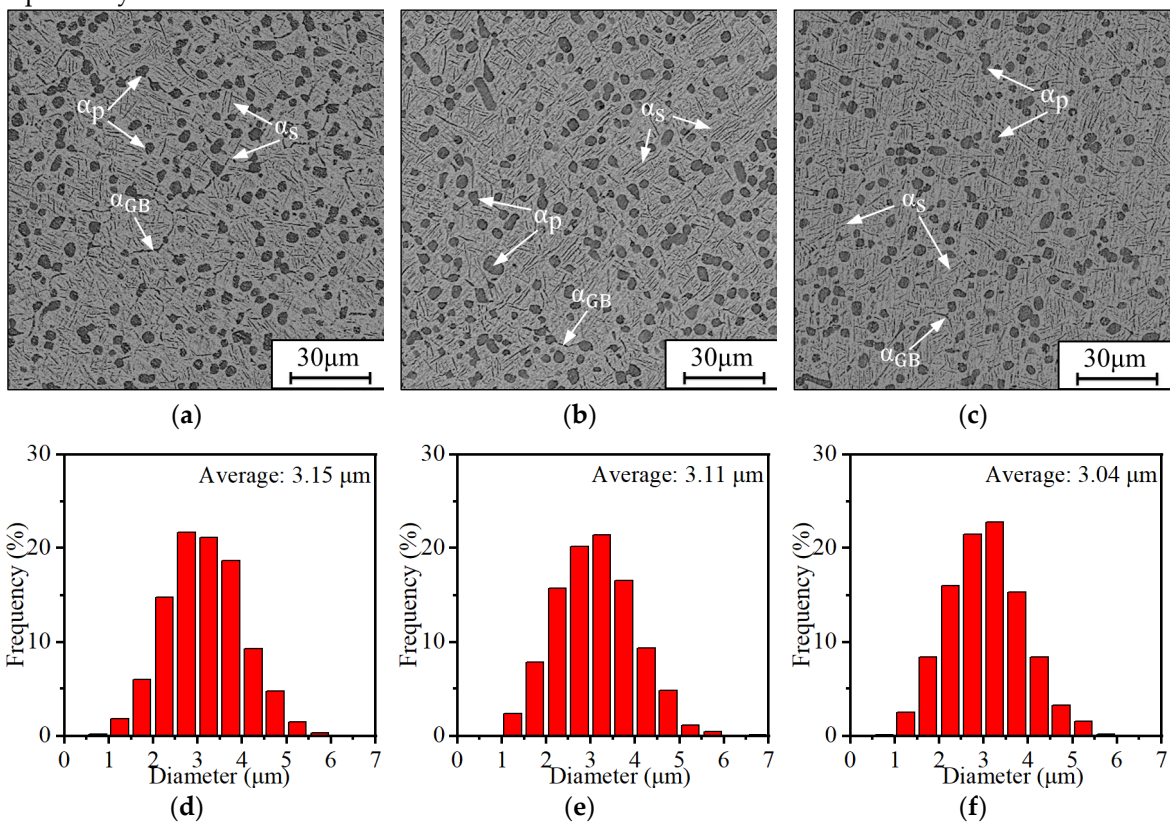

Figure 4. Microstructures and size distributions of α_p phases after aged at 450 °C and the ageing time of: (**a**), (**d**) 1 h; (**b**), (**e**) 4 h; (**c**), (**f**) 8 h.

Figure 5 shows the influence of ageing time on the α_s phases at different ageing temperatures. At 450 °C, the fine acicular α_s phases appear in β_m when aged for 2 h (Figure 5a). As the ageing time is 4 h, the morphologies of α_s phases change significantly and display a typical coarsening behavior (Figure 5b). At 500 °C, the same experimental results are obtained with increasing the ageing time (Figure 5c,d). At both 450 °C and 500 °C, α_s phases are getting coarser and the spaces between adjacent α_s phases become narrow with increasing the ageing time. Actually, the thickness and interlamellar space of α_s phases are little varied, compared with those results shown in Figure 3. So, it can be concluded that the influence of ageing time on the microstructures is weaker than that of ageing temperature.

Preprints (www.preprints.org) | NOT PEER-REVIEWED | Posted: 3 January 2024 doi:10.20944/preprints202401.0281.v1

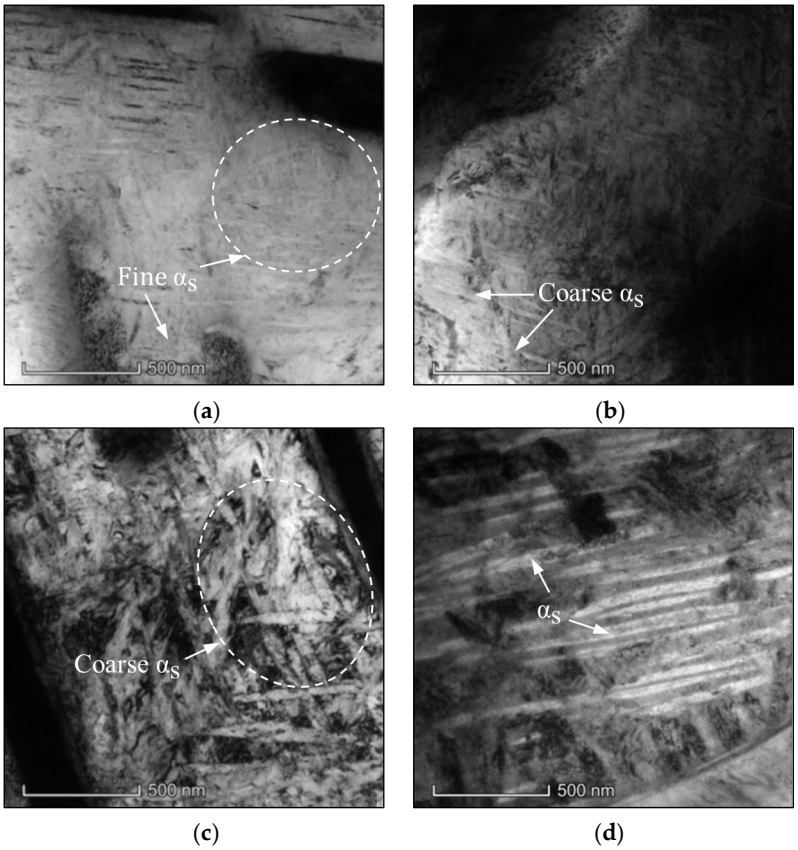

Figure 5. TEM micrographs of TC18 alloy aged at: (**a**) 450 °C/2 h/AC; (**b**) 450 °C/4 h/AC; (**c**) 500 °C/4 h/AC; (**d**) 500 °C/8 h/AC.

3.2. Effects of Ageing Conditions on Tensile Properties

3.2.1. Tensile Properties of the Aged TC18 Alloy

Table 3 gives the tensile properties of TC18 alloy aged at different ageing conditions. It is apparent that both the ageing temperature and time are responsible for the strength and ductility of the aged alloy. Compared with the alloy without ageing treatment, the strength or ductility of the aged alloy has been improved. As the ageing temperature is increased, the strength increases first and then decreases. An excellent balance exists between the strength and ductility of the alloy aged at 450–550 °C. The yield strength (YS) ranges from 1238.6 to 1381.6 MPa, and the ultimate tensile strength (UTS) ranges from 1363.2 to 1516.8 MPa. Also, the moderate elongation (δ) ranges from 9.0% to 10.3%. When aged at 600 °C, the UTS and YS are almost equal to those at 400 °C, while the ductility is obviously different. There is a sharp increase in ductility (~15.1%). Unlike common understandings, only 0.9% loss of the UTS (~12 MPa) can result in a ~34% increase in the elongation of the alloy. To further reveal the influences of ageing time on the properties, the specimens were aged at 450 °C for 2, 4 and 8 h. The UTS and YS are still relatively high (1263.4–1516.9 MPa), while the ductility shows a concave parabolic tendency. In addition, the influence of ageing temperature on tensile properties is more obvious than that of ageing time, which is consistent with those analyses in section 3.1. So, the α_s phases induced by ageing treatment can optimize the properties of TC18 alloy.

Table 3. Tensile properties of the alloy aged for different conditions.

Pre-treatment	Ageing conditions	Yield strength (YS)/MPa	Ultimate tensile strength (UTS)/MPa	Elongation(δ)/%
780 °C/1 h/WQ	/	1220.2	1359.9	9.1
	400 °C/4 h/AC	1157.9	1248.2	11.3
	450 °C/2 h/AC	1263.4	1406.9	12.5

Preprints (www.preprints.org) | NOT PEER-REVIEWED | Posted: 3 January 2024 doi:10.20944/preprints202401.0281.v1

450 °C/4 h/AC	1381.6	1516.8	9.3
450 °C/8 h/AC	1353.7	1516.9	11.2
500 °C/4 h/AC	1358.3	1463.5	9.0
550 °C/4 h/AC	1238.6	1363.2	10.3
600 °C/4 h/AC	1156.8	1236.7	15.1

3.2.2. Effects of microstructural features on tensile properties of the aged TC18 alloy

The experimental findings above reveal the effects of the ageing conditions on microstructures, which results in the difference in properties. In general, the morphologies of α_s phases mainly determine the strengths, and the content of α_p phase and the size of β grain mainly control the ductility of near β-Ti alloys with duplex microstructures [37–39]. Due to all the specimens are pretreated by the same method in this work, the size of β grain is insignificant in discussing the factors affecting the mechanical properties. As a rule, the strength of the near β-Ti alloy increases with decreasing the ageing temperature and time after the solution within α+β region [27,35,38]. The trade-off for an excellent strength is a poor ductility. In fact, some differences with the fore-mentioned standpoints are presented in this work, e.g., both the strengths and ductility decrease (aged at 450 and 500 °C for 4 h). Such slight contradictory phenomena might be a consequence of the competitive effects of the content of α phase and the thickness of α_s phase, i.e., the content of α phase dramatically decreases (27.61%–23.79%) while the thickness of α_s phases slightly increases (0.30 to 0.35 μm shown in Table 2). The detailed changing trend of feature parameters are summarized in Table 4. The tensile strengths and ductility at the ageing temperature of 500 °C are slightly reduced, compared those at 450 °C. Furthermore, the tensile strength continually decreases with increasing the content of α phase or the thickness of α_s phase when the ageing temperature exceeds 500 °C (Table 4).

Table 4. Tensile properties of the alloy aged for different conditions.

Temperature	The content of α phases	The thickness of α_s phases	The tensile strength	Ductility
450→500 °C	↓	↑	↓	↓
500→550 °C	↑	↑	↓	↑
550→600 °C	↓	↑	↓	↑

The symbols "↑" and "↓" represent the increase and decrease, respectively.

As described above, the fine acicular α_s phases precipitate in the β_m during ageing treatment at low temperatures such as 400 and 450 °C. These acicular α_s phases can create massive phase boundaries that act as dislocation barriers and effectively block the dislocations at interfaces. Thus, the strength increases. Nevertheless, the strength of the alloy aged at 450 °C is better than that aged at 400 °C. In fact, although the size of precipitated α_s phases is extremely fine when aged at 400 °C, its content is low due to the lower diffusion driving force. Therefore, the strength is lower than that aged at 450 °C. It must be mentioned that α_s phases become coarse with increasing the temperature and time. These coarse α_s phases increase the slip distance of dislocations while decrease the number of α/β phase boundaries. So, the strength decreases with increasing the temperature and time. As indicated in the other report [40], the cavities are formed at α/β phase interfaces during plastic deformation. Moreover, the cavities grow along with the α/β interfaces and coarsen or gather to form microcracks. The free path of the cavities growing and the micro-cracks is hindered by α phases. Therefore, the more α phases are, the shorter the free path is. These cavities encounter more obstacles in the growing progress [15], which improves the ductility. In addition, the dislocations are activated at α/β interfaces and firstly slip in α phases with a lower resolved shear stress [30]. An increasing content of α phase can increase the degree of uniform plastic deformation and thus improves the ductility. Also, the mean-free-path of dislocations (or slip) increases with increasing the sizes of α_s phases [22]. Especially at 600 °C, the content of α phase tends to be stable (~26%), but the ductility still is better than that aged at 550 °C. This is a result of the coarsening and homogenization of α_s phase. Therefore, the coarse α_s phases induced by increasing the temperature and time can contribute

Preprints (www.preprints.org) | NOT PEER-REVIEWED | Posted: 3 January 2024 doi:10.20944/preprints202401.0281.v1

to the improvement of ductility. In short, the thickness of α_s phase is responsible for the strength, while the content of α phase can enhance the ductility.

3.2.3. Crucial roles of affecting tensile strengths for TC18 alloy

The properties of Ti alloys are bound up with the microstructural features [31,41,42], e.g., the content of α phase, the size of β grain, the diameter of α_p grain and the thickness of α_s phase. In this work, the classical Hall-Petch formula is employed to express the YS or UTS [35,43],

$$\sigma_i = \sigma_s + k_i^A v_\beta d_\beta^{-1/2} + k_i^B v_{\alpha_p} d_{\alpha_p}^{-1/2} + k_i^C v_{\alpha_s} l_{\alpha_s}^{-1/2} \left(i = \text{YS, UTS}\right) \quad (1)$$

where σ_i are the strengths (YS or UTS), σ_s represents the total resistance determined by the crystalline structure and the dislocation density, k_i^A, k_i^B and k_i^C are the pin constant of β grain, α_p and α_s phases, respectively. v denotes the content or volume fraction of β grain, α_p or α_s phases, d represents the diameter of grain and l is the thickness of lamellar α_s phase.

In the present work, all specimens undergo the same solution treatment. Synthesizing the previous analysis, the involved eigenvalue of β grains and α_p phases are regarded as constant. So, σ_i can be rewritten as,

$$\sigma_i = f\left(v_{\alpha_s} l_{\alpha_s}^{-1/2}\right) + C \quad (2)$$

where f is a linear function of the eigenvalue v_{α_s} and $l_{\alpha_s}^{-1/2}$, C represents a constant.

From Equation (2), it is apparently manifest that the suitable approach for improving the strength is increasing the volume fraction of α_s phase or decreasing the thickness of α_s phase. Figure 6 depicts the relationship between the strengths and key factor involving α_s phases. When the volume fraction of α_s phase is not considered, a good linear correlation exists between the strengths and the reciprocal square root of the thickness of α_s phase (Figure 6a). Meanwhile, a non-linear relation exists between the strengths, the product of v_{α_s} and the reciprocal square root of α_s thickness l (Figure 6b). The results indicate that decreasing the thickness of α_s phase can improve the strengths, and the thickness of α_s phase is a key factor affecting the strengths of TC18 alloy with duplex microstructures. The conclusions are also consistent with the experimental findings of Mora [39].

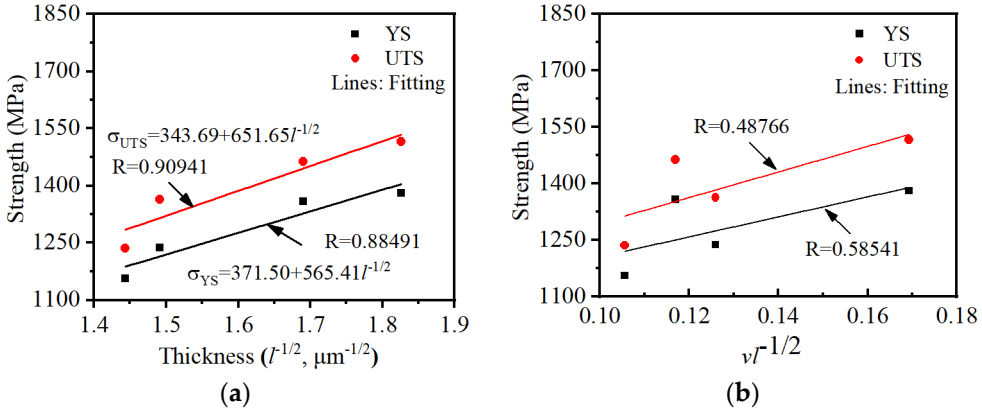

Figure 6. The relationship between the strengths and key factor involving α_s phases: (**a**) $\sigma_i - l_{\alpha_s}^{-1/2}$; (**b**) $\sigma_i - v_{\alpha_s} l_{\alpha_s}^{-1/2}$.

In summary, the thin α_s phases with large aspect ratio precipitate at low ageing temperatures, which results in a high interface energy and external energy for plastic deformation [35]. The tensile strengths are excellent while the poor ductility appears. The α_s phases are coarse and shorter, which reduces the required external energy for plastic deformation. Thus, the strength decreases while the ductility increases at high ageing temperatures.

3.3. Fractographies and Fracture Mechanisms

3.3.1. Fractographies of TC18 alloy

Preprints (www.preprints.org) | NOT PEER-REVIEWED | Posted: 3 January 2024 doi:10.20944/preprints202401.0281.v1

The macroscopic fractures of the alloy at the ageing temperatures from 450 to 600 °C are illustrated in Figure 7. It can be noted that the surface roughness of fractures is quite different at the 4 ageing paths. The surface morphologies vary from the flatness to the roughness with increasing the temperature. In particular, there are large undulating ravines on the fracture surface at 600 °C (Figure 7d), which indicates the excellent ductility (~15.1%). The tensile fracture surfaces can be divided into two distinct zones: fibrous and shear lip zone [44,55]. Figure 8 shows the microscopic images of fibrous zone. Fracture surfaces under different ageing conditions contain some dimples but their sizes are unhomogeneous. The diameters of unhomogeneous irregular dimples are approximately 0.2-6.0 μm. What's more, a great deal of tear ridges and some facets gather around dimples. The proportion of unhomogeneous dimples is lower at lower temperatures (Figure 8a,b), but increases at higher temperatures (Figure 8c,d). Moreover, these unhomogeneous dimples in Figure 8a,b are shallower than those in Figure 8c,d.

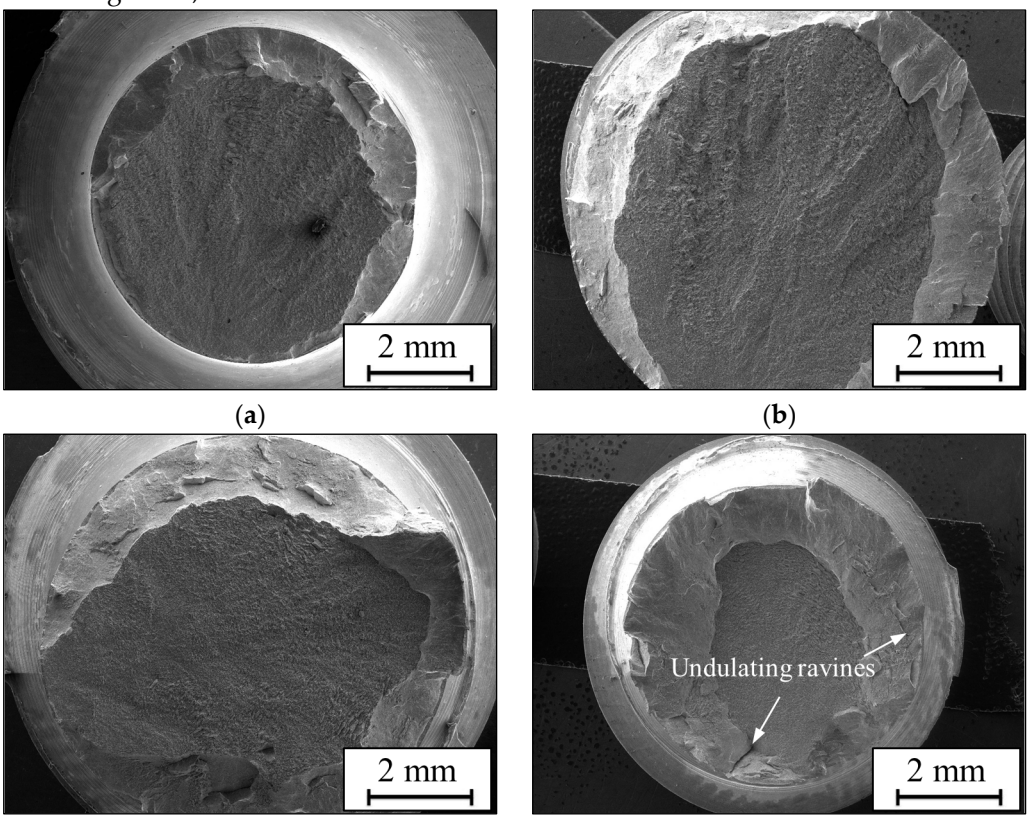

Figure 7. The macroscopic fracture of TC18 alloy aged at: (**a**) 450 °C; (**b**) 500 °C; (**c**) 550 °C; (**d**) 600 °C.

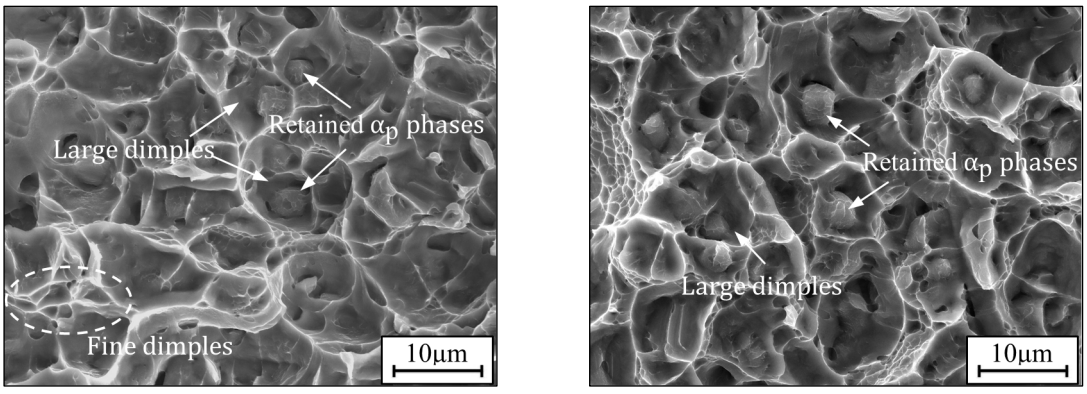

Preprints (www.preprints.org) | NOT PEER-REVIEWED | Posted: 3 January 2024 doi:10.20944/preprints202401.0281.v1

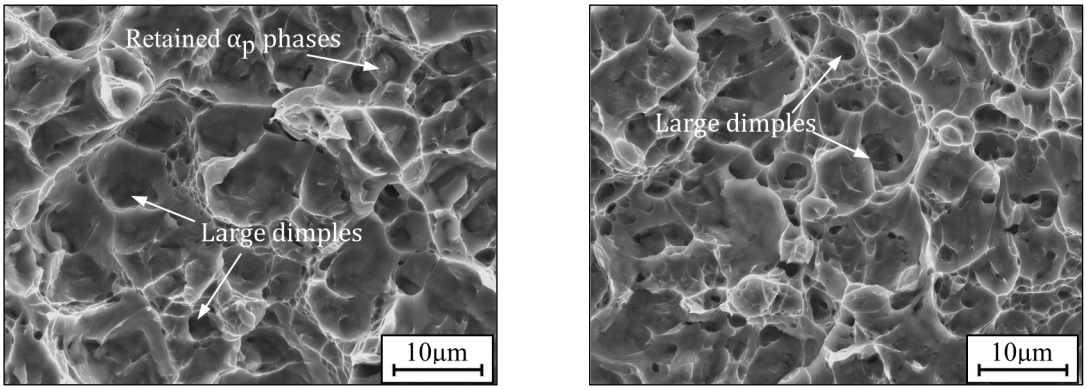

(**c**) (**d**)

Figure 8. The microscopic fracture morphologies of TC18 alloy aged at: (**a**) 450 °C; (**b**) 500 °C; (**c**) 550 °C; (**d**) 600 °C.

3.3.2. Fracture Mechanisms

Usually, the fracture behavior of TC18 alloy is inextricable to microstructures. Tensile fracture failures of the alloy aged at different conditions are mixed-mode, including a quasi-cleavage and ductile failure. However, the fracture surface roughness and morphologies among 4 ageing routes are quite different. In addition, the degree of necking also varies dramatically. The fracture surface at 450 °C is flat (Figure 7a), and the surfaces become rougher with increasing the average thickness of α_s phase (Figure 7c,d). A lot of unhomogeneous cavities that nucleate and coarsen along with the interface of α phase and β_m induce the fracture failure of the studied alloy [46]. References [44] and [47] indicated that the interfaces of α_p/β_m phase are easy to be the potential nucleation site of micro-voids due to the difficulty in coordinating deformation. The bottom sizes of these large dimples are approximately equal to the diameter of α_p phases (~3 μm). Some equiaxed α_p phases are retained at the bottom of dimples after fracture (Figure 8a–c). Although the retained α_p phases are not visible in Figure 8d, these large dimples are still induced by nucleation and coarsening at the α_p/β_m interfaces. Moreover, some fine dimples exist around the large dimples (Figure 8a), and the size of fine dimple approximately is equal to the thickness of α_s phase. Because of the small thickness, α_s phases hardly accommodate the plastic deformation. Thus, there are fewer dimples left after fracture (Figure 8a,b). However, the sizes of dimples induced by α_s phases gradually increase with increasing the temperature (Figure 8c,d), which indicates that the coarsening of α_s phases makes a certain contribution to enhance the ductility. The data shown in Table 3 also verify this conclusion. In addition, α_s phases weave tightly in β_m with increasing the temperature or time (Figure 3 and 5), and the crack cannot avoid encountering coarse α_s phases during propagation. Thus, a larger plastic deformation zone will form nearby the crack tip of coarse α_s phases than those with no α_s phases or finer α_s phases in β_m [20]. All aforementioned consequences result in the phenomenon that the ductile failure characters of the alloy with coarser α_s phases are more obvious than those with thinner α_s phases. Therefore, it is feasible to enhance the ductility of TC18 alloy by controlling the proper ageing conditions to coarsen α_s phases.

4. Conclusions

The influences of ageing conditions on microstructures and properties of TC18 alloy were systematically investigated. The crucial conclusions are shown below.

1. α_p phases are insensitive to the ageing temperature and time. However, the temperature and time significantly affect α_s phases. The fine acicular α_s phases precipitate in β_m during ageing treatments and become coarsen with increasing the temperature or time.

2. The thickness of α_s phases is responsible for the strengths while the content of α phases can enhance the ductility. Nevertheless, an excellent balance exists between strengths and ductility, particularly aged at 450–550 °C. The YS ranges from 1238.6 to 1381.6 MPa, and the UTS ranges from 1363.2 to 1516.8 MPa with the moderate elongations ranging from 9.0% to 10.3%.

3. The failures of the alloy aged under different conditions are mixed-mode, including a quasi-cleavage and ductile failure. The ductile fracture characteristics of the alloy with coarser α_s phases are more obvious than those with thinner α_s phases. Consequently, the coarsening of α_s phases makes a certain contribution to improve the ductility of TC18 alloy with duplex microstructures.

Author Contributions: S.Z.: Data curation, Investigation, Writing-original draft, Writing-review & editing, Methodology. Y.-C.L.: Conceptualization, Methodology, Supervision, Writing-review & editing. L.-H.W.: Data curation, Investigation. H.-B.D.: Data curation, Investigation. Y.-L.Q.: Data curation, Investigation. All authors have read and agreed to the published version of the manuscript.

Funding: This work was supported by the National Key Research and Development Program of China (No. 2022YFB3706901), and the Fundamental Research Funds for the Central Universities of Central South University (Grant No. 2022ZZTS0180), China.

Institutional Review Board Statement: Not applicable.

Informed Consent Statement: Not applicable.

Data Availability Statement: The raw/processed data required to reproduce these findings cannot be shared at this time as the data also form part of an ongoing study.

Conflicts of Interest: The authors declare no conflicts of interest.

References

1. Xiao, Y.W.; Lin, Y.C.; Jiang, Y.Q.; Zhang, X.Y.; Pang, G.D.; Wang, D.; Zhou, K.C. A dislocation density-based model and processing maps of Ti-55511 alloy with bimodal microstructures during hot compression in α+β region. *Mater. Sci. Eng. A* **2020**, 790, 139692.
2. Gao, P.; Zhu, Y.X.; Zhu, J.C.; Wang, C.W.; Liu, X.; Han, K.N.; Wang, B.W.; Yang, Q.; Bai, C.Y. Studies on the life, damage evolution, and crack propagation behaviors of TC18 titanium alloy under repeated impact loading. *Int. J. Fatigue* **2024**, 179, 108074.
3. Abbasi, S.M.; Morakkabati, M.; Sheikhali, A.H.; Momeni, A. Hot deformation behavior of beta titanium Ti-13V-11Cr-3Al alloy. *Metall. Mater. Trans. A* **2014**, 45, 5201–5211.
4. Momeni, A.; Abbasi, S.M.; Sadeghpour, S. A comparative study on the hot deformation behavior of Ti-5Al-5Mo-5V-3Cr and newly developed Ti-4Al-7Mo-3V-3Cr alloys. *Vacuum* **2019**, 161, 410–418.
5. Wang, Q.W.; Lin, Y.C.; Jiang, Y.Q.; Liu, X.G.; Zhang, X.Y.; Chen, D.D.; Chen, C.; Zhou, K.C. Precipitation behavior of a β-quenched Ti-5Al-5Mo-5V-1Cr-1Fe alloy during high-temperature compression. *Mater. Charact*. **2019**, 151, 358–367.
6. Zhao, Q.Y.; Yang, F.; Torrens, R.; Bolzoni, L. Evaluation of the hot workability and deformation mechanisms for a metastable beta titanium alloy prepared from powder. *Mater. Charact*. **2019**, 149, 226–238.
7. Mandal, S.; Gockel, B.T.; Balachandran, S.; Banerjee, D.; Rollett, A.D. Simulation of plastic deformation in Ti-5553 alloy using a self-consistent viscoplastic model. *Int. J. Plast.* **2017**, 94, 57–73.
8. Elshaer, R.N.; El-Hadad, S.; Nofal, A. Influence of heat treatment processes on microstructure evolution, tensile and tribological properties of Ti6Al4V alloy. *Sci. Rep*. **2023**, 13, 1–20.
9. Dong, Y.; Liu, X.G.; Xu, H.; He, Y.N.; Ke, Y.J.; Zhang, W.W. Relationship between B→α dynamic transformation and dynamic recrystallization under thermomechanical coupling in Ti-5Al-5Mo-5V-1Cr-1Fe alloy. *J. Mater. Sci. Technol.* **2024**, 179, 98–113.
10. Bobbili, R.; Ramudu, B.V.; Madhu, V. A physically-based constitutive model for hot deformation of Ti-10-2-3 alloy. *J. Alloys Compd.* **2017**, 696, 295–303.
11. Yasmeen, T.; Rahimi, S.; Hopper, C.; Zhang, C.; Jiang, J. Unravelling thermal-mechanical effects on microstructure evolution under superplastic forming conditions in a near alpha titanium alloy. *J. Mater. Res. Technol*. **2022**, 18, 4285–4302.
12. Wen, D.X.; Zhang, M.; Xiong, Y.B.; Wang, W.H.; Li, J.J. Constitutive modeling hot tensile behavior of Ti6Al4V alloy by considering phase transformation and damage mechanisms. *Mater. Sci. Eng. A* **2023**, 890, 145887.
13. Prakash, P.S.L.; Rakshit, R.; Mandal, S.; Gopal Roy, G.; Panda, S.K. Uniaxial tensile deformation behaviour of electron beam welded commercially pure titanium and Ti6Al4V joints: experimental and metallurgical characterization. *J. Manuf. Process.* **2022**, 76, 444–456.
14. Zhang, C.J.; Jiang, X.; Han, J.C.; Zhang, S.Z.; Peng, P.; Feng, H.; Wang, T.; Cao, P. Probing the texture transition sequence of near β titanium matrix composites by observing the uneven hot deformation microstructure. *Mater. Charact.* **2023**, 198, 112728.
15. Guo, P.; Zhao, Y.Q.; Zeng, W.D.; Hong, Q. The effect of microstructure on the mechanical properties of TC4-DT titanium alloys. *Mater. Sci. Eng. A* 792 (2020) 139822. **2013**, 563, 106–111.

16. Yu, Y.B.; Yan, H.G.; Zhu, H.M.; Chen, J.H.; Xia, W.J.; Sun, Y.P.; Su, B.; Deng, Y.F.; Song, M. Dynamic recrystallization behavior and mechanism of bimodal TC17 titanium alloy during high strain rate hot compression. *Mater. Today Commun.* **2023**, 34, 105255.
17. Saboori, A.; Abdi, A.; Fatemi, S.A.; Marchese, G.; Biamino, S.; Mirzadeh, H. Hot deformation behavior and flow stress modeling of Ti-6Al-4V alloy produced via electron beam melting additive manufacturing technology in single β-phase field. *Mater. Sci. Eng. A* **2020**, 792, 139822.
18. Jiang, Y.Q.; Lin, Y.C.; Zhao, C.Y.; Chen, M.S.; He, D.G. A new method to increase the spheroidization rate of lamellar α microstructure during hot deformation of a Ti-6Al-4V Alloy. *Adv. Eng. Mater.* **2020**, 22.
19. Wang, J.; Lin, X.; Wang, J.T.; Yang, H.; Zhou, Y.H.; Wang, C.; Li, Q.G.; Huang, W.D. Grain morphology evolution and texture characterization of wire and arc additive manufactured Ti-6Al-4V. *J. Alloys Compd.* **2018**, 768, 97–113.
20. He, S.T.; Zeng, W.D.; Xu, J.W.; Chen, W. The effects of microstructure evolution on the fracture toughness of BT-25 titanium alloy during isothermal forging and subsequent heat treatment. *Mater. Sci. Eng. A* **2019**, 745, 203–211.
21. Ahmed, M.; Savvakin, D.G.; Ivasishin, O.M.; Pereloma, E.V. The effect of ageing on microstructure and mechanical properties of powder Ti-5Al-5Mo-5V-1Cr-1Fe alloy. *Mater. Sci. Eng. A* **2014**, 605, 89–97.
22. He, D.G.; Su, G.; Lin, Y.C.; Jiang, Y.Q.; Li, Z.; Chen, Z.J.; Yan, X.T.; Xia, Y.C.; Xie, Y.C. Microstructural variation and a physical mechanism model for a Ti-55511 alloy during double-stage hot deformation with stepped strain rates in the β region. *Materials* **2021**, 14, 6371.
23. Jia, R.C.; Zeng, W.D.; Zhao, Z.B.; Wang, S.M.; Xu, J.W.; Wang, Q.J. Growth mechanism of α_p and interface relationships between α_p and α_s during cooling of a near α titanium alloy. *Mater. Des.* **2022**, 223, 111191.
24. Lypchanskyi, O.; Śleboda, T.; Łukaszek-Sołek, A.; Zyguła, K.; Wojtaszek, M. Application of the strain compensation model and processing maps for description of hot deformation behavior of metastable β titanium alloy. *Materials* **2021**, 14, 2021.
25. Dong, J.Z.; Li, F.G.; Wang, C.P. Micromechanical behavior study of α phase with different morphologies of Ti-6Al-4V alloy by microindentation. *Mater. Sci. Eng. A* **2013**, 580, 105–113.
26. Ren, L.; Xiao, W.L.; Chang, H.; Zhao, Y.Q.; Ma, C.L.; Zhou, L. Microstructural tailoring and mechanical properties of a multi-alloyed near β titanium alloy Ti-5321 with various heat treatment. *Mater. Sci. Eng. A* **2018**, 711, 553–561.
27. Lin, Y.C.; Pang, G.D.; Jiang, Y.Q.; Liu, X.G.; Zhang, X.Y.; Chen, C.; Zhou, K.C. Hot compressive deformation behavior and microstructure evolution of a Ti-55511 alloy with basket-weave microstructures. *Vacuum* **2019**, 169, 108878.
28. Liu, C.; Zhou, G.; Wang, X.; Liu, J.J.; Li, J.L.; Zhang, H.Y.; Chen, L.J. Rheological law and mechanism for superplastic deformation of Ti-6Al-4V. *Materials* **2019**, 12, 3520.
29. Shekhar, S.; Sarkar, R.; Kar, S.K.; Bhattacharjee, A. Effect of solution treatment and aging on microstructure and tensile properties of high strength β titanium alloy, Ti-5Al-5V-5Mo-3Cr. *Mater. Des.* **2015**, 66, 596–610.
30. Santhosh, R.; Geetha, M.; Saxena, V.K.; Nageswararao, M. Studies on single and duplex aging of metastable beta titanium alloy Ti-15V-3Cr-3Al-3Sn. *J. Alloys Compd.* **2014**, 605, 222–229.
31. Long, W.; Zhang, S.; Liang, Y.L.; Ou, M.G. Influence of multi-stage heat treatment on the microstructure and mechanical properties of TC21 titanium alloy. *Int. J. Miner. Metall. Mater.* **2020**, 28, 1–9.
32. Yadav, P.; Saxena, K.K. Effect of heat-treatment on microstructure and mechanical properties of Ti alloys: An overview. *Mater. Today Proc.* **2019**, 26, 2546–2557.
33. Aeby-Gautier, E.; Denand, B.; Teixeira, J.; Dehmas, M.; Appolaire, B.; Settefrati, A. Influence of microstructure on tensile properties of β-metastable Ti 17 alloy. *12th World Conf. Titan. (Ti-2011)* **2012**, 2, 1191–1195.
34. Qi, L.; He, S.Y.; Chen, C.J.; Jiang, B.B.; Hao, Y.L.; Ye, H.Q.; Yang, R.; Du, K. Diffusional-displacive transformation in a metastable β titanium alloy and its strengthening effect. *Acta Mater.* **2020**, 195, 151–162.
35. Wu, C.; Zhan, M. Microstructural evolution, mechanical properties and fracture toughness of near β titanium alloy during different solution plus aging heat treatments. *J. Alloys Compd.* **2019**, 805, 1144–1160.
36. Fan, J.K.; Li, J.S.; Kou, H.C.; Hua, K.; Tang, B.; Zhang, Y.D. Influence of solution treatment on microstructure and mechanical properties of a near β titanium alloy Ti-7333. *Mater. Des.* **2015**, 83, 499–507.
37. Lin, Y.C.; Wu, Q.; Pang, G.D.; Jiang, X.Y.; He, D.G. Hot tensile deformation mechanism and dynamic softening behavior of Ti-6Al-4V alloy with thick lamellar microstructures. *Adv. Eng. Mater.* **2020**, 22, 1901193.
38. Elshaer, R.N.; Ibrahim, K.M. Effect of cold deformation and heat treatment on microstructure and mechanical properties of TC21 Ti alloy. *Trans. Nonferrous Met. Soc. China* **2020**, 30, 1290–1299.
39. Mora, L.; Quesne, C.; Penelle, R. Microstructure, and tensile properties of a near beta-titanium treatments and tensile properties. *J. Mater. Res.* **1996**, 12, 89–99.
40. Bantounas, I.; Dye, D.; Lindley, T.C. The Role of microtexture on the faceted fracture morphology in Ti-6Al-4V subjected to high-cycle fatigue. *Acta Mater.* **2010**, 58, 3908–3918.

41. Lin, Y.C.; Wang, L.H.; Wu, Q.; Xiao, Y.W.; Cheng, H.; Zhang, X.Y. Effects of solution temperature and cooling rate on α phases and mechanical properties of a forged Ti-55511 alloy. *Mater. Res. Express* **2019**, 6, 1165h2.
42. Zhu, Z.G.; Ng, F.L.; Seet, H.L.; Nai, S.M.L. Tailoring the microstructure and mechanical property of laser powder bed fusion fabricated Ti-6Al-2Sn-4Zr-2Mo via heat treatment. *J. Alloys Compd.* **2022**, 895, 162648.
43. Wen, X.; Wan, M.P.; Huang, C.W.; Lei, M. Strength and fracture toughness of TC21 alloy with multi-level lamellar microstructure. *Mater. Sci. Eng. A* **2019**, 740–741, 121–129.
44. Qin, D.Y.; Lu, Y.F.; Guo, D.Z.; Zheng, L.; Liu, Q.; Zhou, L. Tensile deformation and fracture of Ti-5Al-5V-5Mo-3Cr-1.5Zr-0.5Fe alloy at room temperature. *Mater. Sci. Eng. A* **2013**, 587, 100–109.
45. Ma, W.; Liu, S.G.; Zhang, X.; Chen, B.H.; Wang, F.; Zhang, X.Y.; Ma, M.Z.; Liu, R.P. Microstructural evolution and mechanical properties of hot-rolled Ti-30Zr-5Al-2.5Sn alloy with mixed α and α' phases. *Mater. Sci. Eng. A* **2020**, 792, 139812.
46. Huang, C.W.; Zhao, Y.Q.; Xin, S.W.; Zhou, W.; Li, Q.; Zeng, W.D. Effect of microstructure on tensile properties of Ti-5Al-5Mo-5V-3Cr-1Zr alloy. *J. Alloys Compd.* **2017**, 693, 582–591.
47. Bieler, T.R.; Fallahi, A.; Ng, B.C.; Kumar, D.; Crimp, M.A.; Simkin, B.A.; Zamiri, A.; Pourboghrat, F.; Mason, D.E. Fracture initiation/propagation parameters for duplex TiAl grain boundaries based on twinning, slip, crystal orientation, and boundary misorientation. *Intermetallics* **2005**, 13, 979–984.